3D nanoparticle superlocalization with a thin diffuser

Tengfei Wu, Marc Guillon, Clemence Gentner, Herve Rigneault, Gilles Tessier, Pierre Bon, Pascal Berto

▶ **To cite this version:**

Tengfei Wu, Marc Guillon, Clemence Gentner, Herve Rigneault, Gilles Tessier, et al.. 3D nanoparticle superlocalization with a thin diffuser. Optics Letters, 2022, 47 (12), pp.3079. 10.1364/OL.453813 . hal-03782304

HAL Id: hal-03782304
https://hal.science/hal-03782304

Submitted on 21 Sep 2022

HAL is a multi-disciplinary open access archive for the deposit and dissemination of scientific research documents, whether they are published or not. The documents may come from teaching and research institutions in France or abroad, or from public or private research centers.

L'archive ouverte pluridisciplinaire **HAL**, est destinée au dépôt et à la diffusion de documents scientifiques de niveau recherche, publiés ou non, émanant des établissements d'enseignement et de recherche français ou étrangers, des laboratoires publics ou privés.

3D nanoparticle superlocalization with a thin diffuser

TENGFEI WU,[1,2] MARC GUILLON,[2,3] CLEMENCE GENTNER[1], HERVE RIGNEAULT,[4] GILLES TESSIER,[1] PIERRE BON,[5] PASCAL BERTO[1,2*]

[1]*Sorbonne Université, CNRS, INSERM, Institut de la Vision, 17 Rue Moreau, 75012 Paris, France*
[2]*Université de Paris, SPPIN – Saints-Pères Paris Institute for the Neurosciences, CNRS, 75006 Paris, France*
[3]*Institut Universitaire de France (IUF), Paris, France*
[4]*Aix Marseille Univ, CNRS, Centrale Marseille, Institut Fresnel, Marseille, France*
[5] *Institut d'Optique, CNRS, LP2N UMR 5298, Université de Bordeaux, UMR 5298, 33400, Talence, France*
**Corresponding author: pascal.berto@u-paris.fr*

Received XX Month XXXX; revised XX Month, XXXX; accepted XX Month XXXX; posted XX Month XXXX (Doc. ID XXXXX); published XX Month XXXX

We report on the use of a thin diffuser placed in the close vicinity of a camera sensor as a simple and effective way to superlocalize plasmonic nanoparticles in 3D. This method is based on holographic reconstruction *via* quantitative phase and intensity measurements of a light field after its interaction with nanoparticles. We experimentally demonstrate that this thin-diffuser can be a simple add-on to a standard bright-field microscope to allow the localization of 100nm gold nanoparticles at video-rate with nanometer precision (1.3nm laterally, and 6.3nm longitudinally). We exemplify the approach by revealing the dynamic Brownian trajectory of a gold nanoparticle trapped in various pockets within an agarose gel. The proposed method provides a simple but highly performant way to track nanoparticle in 3D. © 2021 Optical Society of America

Nanoparticle (NP) tracking with precision beyond the diffraction limit is crucial to many research areas: it is a powerful tool to investigate (electro)chemical reaction[1], study cellular NP pathways[2] or provide insight into motor protein dynamics[3]. The superlocalization of nanoprobes undergoing Brownian motion can also bring a precise stochastic mapping of structures[4] or optical near-field[5]. Owing to their nanometer precision, these techniques can also be used to correct the 3D drift of samples on which NPs are immobilized, thus supporting the performances of super-resolution microscopy techniques[6].

While 2D super-localization in the lateral plane can be easily achieved with a high precision (<10nm) using a conventional 2D Gaussian fit[7] of the Point Spread function (PSF), super-localization along the axial direction requires more complex methods[8]. The most accessible techniques, based on PSF engineering, provide axial localization with typical accuracies of a few tens of nanometers[9,10] but their performances degrade with depth due to the inherent optical aberrations[11]. Better axial precision, 20 nm or below, and better robustness to aberrations can be obtained using Digital Holographic microscopy[5] (DHM), which gives access to the full scalar Electromagnetic field, i.e. amplitude and phase: numerical propagation then allows a precise estimation of NP position in a wide axial range. However, DHM is sensitive to coherence artifacts and relies on a reference arm which hampers its integration to microscopes and increases its sensitivity to vibrations.

WaveFront Sensing (WFS) tends to emerge as less cumbersome and more robust than DHM: self-referenced WFS techniques able to operate with temporally incoherent light, including fluorescence or a native microscope illumination, can become mere add-ons to most commercial microscopes. Shack-Hartmann (SH) and Quadriwave Lateral Shearing Interferometry[12] (QLSI) are the most common WFS techniques. Both are based on an amplitude and/or phase-encoding element placed before a camera. While the use of SH in imaging is limited by the number of microlenses, QLSI can achieve much higher spatial resolution. In this context, we recently demonstrated that QLSI can yield accurate 3D super-localization of immobilized metal NPs and greatly enhance super-resolution microscopy[6]. However, QLSI requires lithographic fabrication of an optimized nanometer-precision phase and amplitude mask (Modified Hartmann Mask) which severely hampers the dissemination of the technique. Consequently, in spite of its weaker performances, astigmatism-based PSF engineering remains the most spread technique for longitudinal localization, owing to its relative simplicity, cost, and to the broad availability of its components.

Following major progresses in the optical description of complex, scattering media, thin diffusers have recently attracted much attention. Owing to their limited thickness, thin diffusers exhibit a large angular "memory effect" [13], i.e. a high correlation of scattered light patterns over a broad range of illumination angles. This property makes them suitable for imaging, including computational lensless imaging[14,15], single-shot 3D microscopy[16] and single-shot video[17]. Based on this effect, we recently proposed a WFS scheme based on a simple thin diffuser placed in the close vicinity of a camera[18], and demonstrated that the method allows to quantitatively image the phase of a transparent object with (i) a high resolution (40 kPixels), (ii) a low phase noise (<λ/300), and (iii) using white-light illumination.

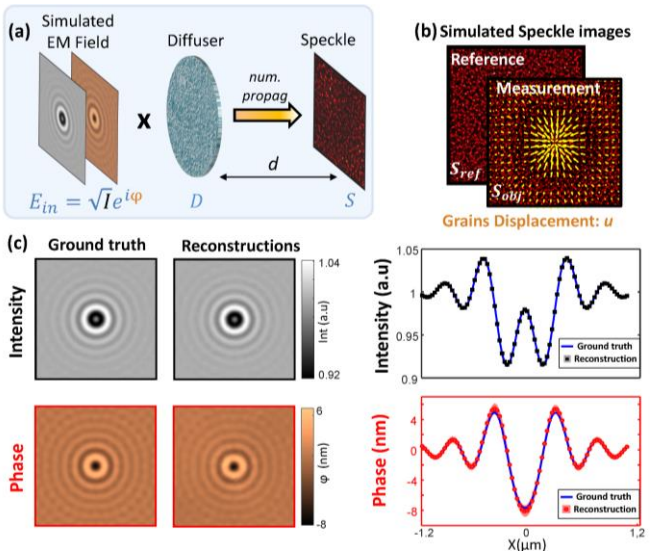

Fig. 1. Technique description based on numerical simulations for phase and intensity reconstruction from speckle images. (a) Modeling of the WFS response: an EM field E_{in} associated to the phase φ and intensity I images of a gold NP (ground truth) is transmitted through a thin diffuser and produces after few mm of propagation (b) a speckle image S_{obj}. A local wavefront distortion produces a speckle grain displacement u (yellow arrows) with respect to a reference speckle pattern (planar wavefront), from which both the intensity and phase can be deduced. (c) Reconstruction performances: comparison of the reconstructed phase and intensity images with their ground truth. Corresponding profiles considering 100 random diffusers: mean (dots) and standard deviation (shadow).

In this Letter, we report that this thin diffuser-based solution can quantitatively measure the wavefield (intensity and phase) scattered by a plasmonic NP, and can efficiently localize and track it in 3D with nanometric precision. We propose a solution to extract the intensity and phase which are entangled in the distorted speckle captured by the camera. We base the description of our approach on numerical simulations which allow an easy and precise comparison to a ground truth wavefield, in order to demonstrate its performances. Then, we show experimentally that this method provides the wavefield of light having interacted with a gold NP, allowing its precise 3D localization over a large depth range.

In a preliminary step, we numerically demonstrate that diffuser-based WFS can quantitatively image both the phase and intensity of light coming from an absorbing nano-object. To validate our approach, we first model the scalar EM field $E_{in} = \sqrt{I}e^{i\varphi}$ after interaction with a 100nm gold NP in a transmission microscope as the product of EM-field contributions from elementary z-slices of the sample[19]. As an illustration, we consider here a slightly defocused NP (Δz=400 nm away from best focusing, z=0) imaged at its plasmonic resonance (λ=576 nm) using NA=1.4. The resulting phase φ and intensity I images shown in Fig.1(a, c) will later provide a "ground truth" to assess WFS reconstruction performances. The WFS is based on a 1° holographic diffuser[18] which we model as a complex transmission $D = e^{i\varphi_D}$ (see Supplementary S1). After interaction with the particle, the field E_{in} is transmitted through the diffuser ($E_{dif} = E_{in}D$) and finally Fresnel-propagated to the camera sensor plane, at a distance d. The resulting speckle intensity pattern S_{obj} (see Fig.1(a,b)) therefore reproduces typical speckle patterns observed in the camera plane.

As in any WFS, the distorted pattern S_{obj} must be compared to the reference pattern S_{ref} produced by a planar wavefront to retrieve wavefront distortions. As described in our earlier work[18], the large angular memory of a thin diffuser ensures that the local phase gradient experienced by the beam stays proportional to the local speckle grain displacement vector $\boldsymbol{u}$: $\boldsymbol{\nabla_{\perp}}\varphi = k_0\boldsymbol{u}/d$.

When the intensity is not affected by the sample, a non-rigid image registration algorithm (*e.g.* Demon) can directly extract the speckle grain displacement (see yellow arrows in Fig 1.b) and thus gives access to the phase after 2D integration of its gradients[18].

Whenever the sample affects both the phase and the intensity, I must be estimated to accurately measure wavefront distortions[20]. Indeed, the measured speckle pattern can be approximated by:

$$\boldsymbol{S_{obj}}(\boldsymbol{r}+\boldsymbol{u}) = \boldsymbol{I}(\boldsymbol{r})\boldsymbol{S_{ref}}(\boldsymbol{r}) \quad (1)$$

where r denotes the coordinates in real space. Both the intensity and the phase of the beam are thus encoded in the speckle pattern S_{obj}, but intensity and phase are predominantly encoded in the low and the high spatial spectrum domains, respectively. The intensity pattern I and the distortion map u can then be estimated iteratively (see Supplementary S2 for a detailed description of the reconstruction algorithm). Briefly, at every iteration, the displacement map $\boldsymbol{u}$ is first computed applying the non-rigid registration Demon algorithm to S_{obj} and $I'S_{ref}$ where I' is the intensity modulation estimated at the former step (I' is considered as uniform at the first iteration). The intensity modulation I' is then estimated by (i) registering the distorted speckle pattern S_{obj} to compensate for the phase- induced speckle grain displacements u, and (ii) normalizing this registered speckle pattern S_{obj} by the reference speckle pattern S_{ref} . This intensity computation is achieved in the "low" spatial frequency domain using a convolution/deconvolution step dealing both with registration errors and dark regions of the speckle map (see supplementary S3). The final phase and intensity reconstructions and their profiles are shown in Fig. 1(c), and are in good agreement with the expected (ground truth) intensity and phase. This model clearly confirms that the proposed reconstruction method is an efficient way to measure EM fields coming from nano-objects. It is worth mentioning that the reconstruction of I and φ requires that the imaging PSF be sampled over more than 3 phase pixels. A finer sampling will increase accuracy but reduce the field of view (FOV).

To validate this concept experimentally, we built a setup based on a commercial inverted microscope (Olympus IX-71) with a transmission Köhler illumination described in Fig. 2(a). A small aperture diaphragm (NA_{exc} <0.1) ensures the spatial coherence of the white halogen lamp light while a bandpass filter at λ=576±40nm provides excitation at the NP plasmon resonance. The 100x, NA=1.4 oil immersion objective (Olympus) is associated with a tube lens L_T which provides an extra 1.6 magnification. An additional relay lens assembly (magnification M=5.3) is placed before the 1° scattering angle holographic diffuser (Edmund) to adjust the lateral sampling of the PSF to 4 phase pixels (>3, as discussed above). This means that the PSF spreads over 32x32 camera pixels since a phase pixel corresponds to 8x8 camera pixels in this configuration[18]. A diffuser-camera distance d= 3.9 mm was chosen in order to optimize the resolution-sensitivity tradeoff. Placing the diffuser so close to the sensor (PCO Panda 4.2) was mechanically difficult, so an M=1 magnification (not represented in fig. 2a) was used to reimage the diffuser at a distance d from the camera. This distance d was finely tuned using a micrometer stage.

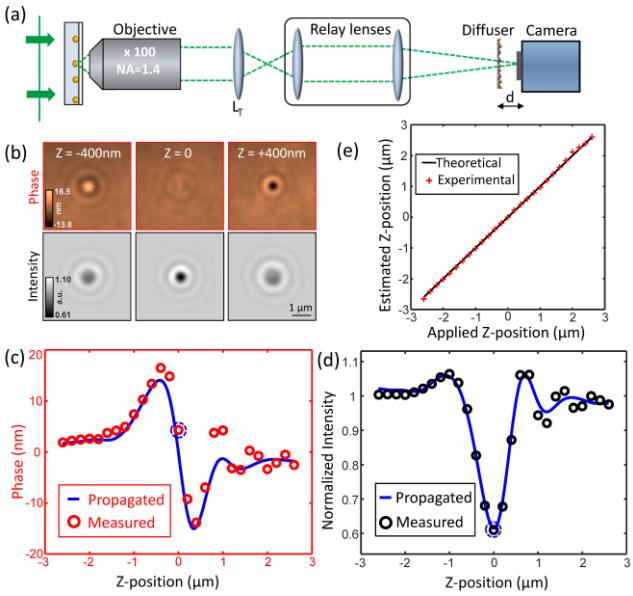

Fig. 2. (a) Experimental setup showing gold NPs imaged on the diffuser-based WFS. (b) Reconstructions of phase and intensity images in various z-planes. (c, d) Experimentally measured phase (red circles) and intensity (black circles) for various z positions. Numerical propagation of the values measured in the z≈0 plane (blue line). Numerical propagation (blue line) computed from measurement at $z_0 \approx 0$ (dashed circle) (e) Comparison of the applied (horizontal axis) and retrieved (vertical) positions.

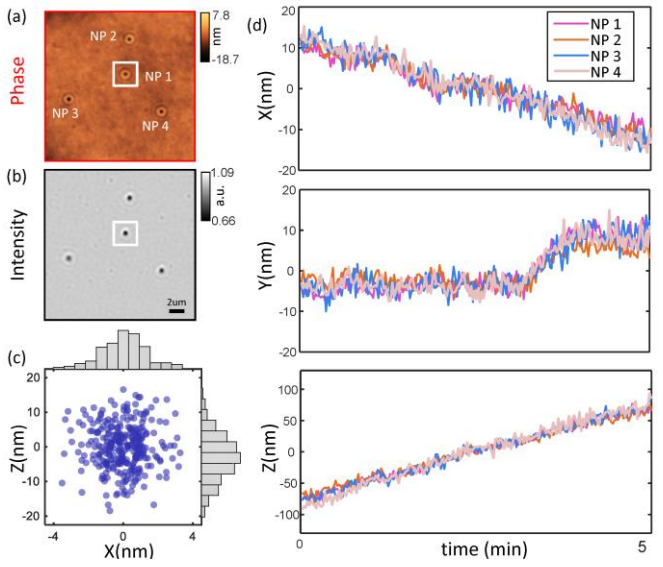

Fig. 3. 3D tracking of immobilized nanoparticles. (a) Phase and (b) intensity extracted from one speckle image. (c) Scatter plot of the X and Z position over time for NP 1 (white square in a and b). After removal of the sample drift contributions, we find a localization precision of 6.3nm in the axial and 1.3nm in the lateral direction (d) 3D tracking of 3 NPs, showing mechanical sample drifts which can be used as input for nanometer-precision sample stabilization.

In order to experimentally validate the axial localization capabilities of the WFS, a drop of water-dispersed 100nm gold NPs (Sigma-Aldrich, #742031) was dried on a microscope slide, and re-immersed in water to obtain immobilized particles in water. A series of displacements along the axial direction were then applied to this sample (from Δz = -2.6 µm to Δz = 2.6 µm in 200nm steps, with z≈0 the imaging plane of the NPs) using a piezo stage (NV 40/1 CL, piezosystem jena). After a reference acquisition without sample, 10 speckle patterns were recorded (~20Hz frame rate) and averaged in each position.

Using the procedure described above, phase and intensity images were reconstructed for each position (see Fig. 2(b)). Their values at the NP center are respectively shown in Fig. 2(c) and 2(d) (circles). While the intensity is symmetric with respect to the optimal focus position (Fig 2d), the phase (Fig 2.c) exhibits sharp variations (which increase z-sensitivity) and a sign inversion (which disambiguates the z-position). Interestingly, since the spatial coherence of the illumination is high as compared to the NA of the objective, numerical propagation of the scalar EM field $E(z_0) = \sqrt{I_{z_0}}.e^{i\varphi_{z_0}}$, measured in the plane $z = z_0$, can be performed to retrieve both the intensity I_z and phase images φ_z in any z-plane. As shown in Fig. 2(c) and 2(d), values calculated in the -2.6µm to 2.6µm range using the $z_0 \approx 0$ plane as a reference position (continuous lines) are in remarkable agreement with those measured using a physical defocusing (circles). This clearly demonstrates that a single speckle measurement contains enough information to accurately reconstruct the full 3D EM field and therefore localize the particle.

At the beginning of the experiment, a first calibration step consists in acquiring one speckle image of a chosen NP and using it to generate by numerical propagation a look-up table of its 3D EM field response $E_{calib}(z)$ with a fine axial sampling (1nm). During the experiment, axial localization is then determined, by choosing the minimal mean-squared error value between the acquired 2D EM field $E(z')$ and its 3D look-up table $E_{calib}(z)$. Using this estimated z-position, the image of the NP can thus be numerically refocused (see Visualization 1) to achieve superlocalization along the X and Y directions using a 2D Gaussian fit (nonlinear Levenberg–Marquardt). To validate the accuracy of the z localization, we applied calibrated piezo stage z-displacements and estimated the NP axial position with the above method. Figure 2(e) shows that accurate axial localization is obtained for defocuses up to 2.6µm, i.e. more than 6 times the incoherent imaging depth-of-field.

In order to quantify the 3D localization precision of the method, 300 speckle images were collected at a high frame rate (20Hz) on immobilized particles. Figure 3(a,b) shows the phase and intensity images reconstructed from one of these measurements. For each frame, all NPs in the FOV were superlocalized in 3D. Figure 3(c) shows a scatter plot of the X and Z positions over time for NP 1 (see Fig 3a). However, this measurement can be affected by vibrations and, although the acquisition is rather short (15 s), by drifts. These were estimated by measuring the correlated part of the displacement of 2 immobilized NPs in the FOV. After correction (see Supplementary S4), we found that this simple diffuser-based WFS can provide a localization precision down to $\sigma_{x,y}$=1.3nm in lateral and σ_z=6.3nm in axial direction when operating close to the plane of best focus. Out of the depth of field (e.g. z=2.6µm), the precision decreases but still remains remarkable ($\sigma_{x,y}$=19nm and σ_z=71nm - see Supplementary S5).

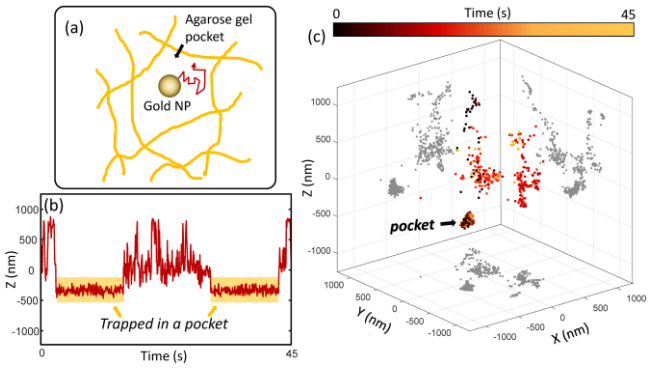

Fig. 4. 3D tracking of the stochastic movements of a 100 nm gold NP in an agarose gel. (a) schematic of an agarose gel pocket containing a single NP. (b) z-coordinates of a moving particle retrieved from speckle patterns during 45 s. (c) 3D representation of the particle positions.

An interesting application of this 3D superlocalization method is the measurement of mechanical and thermal sample drifts. Figure 3(d) shows the 3D tracking of 4 NPs immobilized in the FOV during a 5 min. -long experiment. As discussed above, the precision is in the nm-range and can be improved by averaging the position of several particles, or temporally. This information can be used to correct mechanical/thermal drifts during long experiments, which is essential to applications such as PALM/STORM or nano-lithography.

Having validated the superlocalization capabilities of a thin diffuser-based WFS, we used it to track a moving NP in 3D. 100nm gold NPs were embedded in a 1.33% agarose/water gel. These gels typically feature multiple water pockets in which gold NPs can be trapped (see illustration in Fig. 4(a)). A 45 s-long sequence of speckle patterns was recorded using 5ms exposure times and 15 Hz frame rate. From these data, intensity and phase images were reconstructed, revealing that a single gold NP was present within the FOV. The localization procedure described above was applied to each frame. Figure 4(b) shows the evolution of the z-position of one particle in Brownian motion in the gel. Two regimes are clearly seen, in which the NP either stays confined in a small volume (i.e. trapped in a pocket) or travels stochastically over longer z-distances as shown in Fig. 4(c). At the bottom left, a cluster appears, corresponding to the sequences highlighted in Fig. 4(b), clearly indicating that the nanoparticle was temporarily trapped inside the same pocket twice, and travelled around before, between, and after these events (see Visualization 2). The diameter of this water pocket can be estimated as 350nm, in relatively good agreement with reported agarose/water pockets sizes[21].

We report that a thin diffuser placed in front of a camera allows simultaneous phase and intensity imaging of a single plasmonic NP. While this information is interesting in itself to fully characterize NPs[22], we show that it allows the localization of 100nm gold NPs over a relatively broad range (>5µm). Near the focal plane, we obtain remarkable precisions of 1.3nm in the lateral plane and 6.3nm along the axial direction, precisions which can be adjusted by playing on the magnification of the PSF in the diffuser plane. These performances stand out, particularly if one considers the simplicity, cost efficiency and broad availability of the optical components. These can be assembled into a mere microscope add-on and become (i) a valuable stabilization tool for a variety of super-resolution/nanolithography methods or (ii) an efficient 3D nano-tracking platform for chemistry/biology. While restricted here to the case of Au NPs, this 3D super-localization method could be applied to a broad range of objects, including dielectric NPs (e.g to study vesicle trafficking) or fluorescent molecules (e.g to perform 3D super-resolution[11,23] or tracking[24]).

Funding. Société d'Accélération du Transfert de Technologies - ERGANEO (Project 493); DIM ELICIT - Region Ile de France (3-DiPSI); H2020 European Research Council (848645).

Acknowledgments. The authors thank Photon Lines, to which the technology has been transferred, for the loan of the Panda camera.

Disclosures. The authors declare no conflicts of interest.

Data availability. Data underlying the results presented in this Letter may be obtained from the authors upon reasonable request.

Supplemental document. See Supplement 1 for supporting content.

REFERENCES

1. A. N. Patel, A. Martinez-Marrades, V. Brasiliense, D. Koshelev, M. Besbes, R. Kuszelewicz, C. Combellas, G. Tessier, and F. Kanoufi, Nano Lett. 15, 6454 (2015).
2. M. S. de Almeida, E. Susnik, B. Drasler, P. Taladriz-Blanco, A. Petri-Fink, and B. Rothen-Rutishauser, Chem. Soc. Rev. 50, 5397 (2021).
3. J. Andrecka, J. O. Arroyo, Y. Takagi, G. de Wit, A. Fineberg, L. MacKinnon, G. Young, J. R. Sellers, and P. Kukura, Elife 2015, (2015).
4. M. Gross, F. Verpillat, and P. Desbiolles, BSu3A.62 (2013).
5. A. Martinez-Marrades, J.-F. Rupprecht, M. Gross, and G. Tessier, Opt. Express 22, 29191 (2014).
6. P. Bon, N. Bourg, S. Lécart, S. Monneret, E. Fort, J. Wenger, and S. Lévêque-Fort, Nat. Commun. 6, (2015).
7. H. Lombaert, L. Grady, X. Pennec, N. Ayache, and F. Cheriet, Int. J. Comput. Vis. 107, 254 (2014).
8. B. Hajj, M. El Beheiry, I. Izeddin, X. Darzacq, and M. Dahan, Phys. Chem. Chem. Phys. 16, 16340 (2014).
9. H. P. Kao and A. S. Verkman, Biophys. J. 67, 1291 (1994).
10. B. Huang, W. Wang, M. Bates, and X. Zhuang, Science (80-.). 319, 810 (2008).
11. P. Bon, J. Linarès-Loyez, M. Feyeux, K. Alessandri, B. Lounis, P. Nassoy, and L. Cognet, Nat. Methods 15, 449 (2018).
12. J. Primot and L. Sogno, J. Opt. Soc. Am. A 12, 2679 (1995).
13. S. Feng, C. Kane, P. A. Lee, and A. D. Stone, Phys. Rev. Lett. 61, 834 (1988).
14. T. Wu, O. Katz, X. Shao, and S. Gigan, Opt. Lett. 41, 5003 (2016).
15. N. Antipa, G. Kuo, R. Heckel, B. Mildenhall, E. Bostan, R. Ng, and L. Waller, Optica 5, 1 (2018).
16. F. Linda Liu, G. Kuo, N. Antipa, K. Yanny, and L. Waller, Opt. Express 28, 28969 (2020).
17. X. Li, A. Stevens, J. A. Greenberg, and M. E. Gehm, Sci. Rep. 8, 1 (2018).
18. P. Berto, H. Rigneault, and M. Guillon, Opt. Lett. 42, 5117 (2017).
19. P. Bon, B. Wattellier, and S. Monneret, Opt. Lett. 37, 1718 (2012).
20. C. Wang, Q. Fu, X. Dun, and W. Heidrich, Sci. Rep. 9, (2019).
21. P. N, M. M, and T. B, Electrophoresis 18, 55 (1997).
22. S. Khadir, D. Andrén, P. C. Chaumet, S. Monneret, N. Bonod, M. Käll, A. Sentenac, and G. Baffou, Optica 7, 243 (2020).
23. R. R. Sims, S. Abdul Rehman, M. O. Lenz, S. I. Benaissa, E. Bruggeman, A. Clark, E. W. Sanders, A. Ponjavic, L. Muresan, S. F. Lee, and K. O'Holleran, Optica 7, 1065 (2020).
24. M. Liebel, J. O. Arroyo, V. S. Beltrán, J. Osmond, A. Jo, H. Lee, R. Quidant, and N. F. van Hulst, Sci. Adv. 6, (2020).

Full information of references

1. Patel, A. N., Martinez-Marrades, A., Brasiliense, V., Koshelev, D., Besbes, M., Kuszelewicz, R., Combellas, C., Tessier, G. & Kanoufi, F. Deciphering the Elementary Steps of Transport-Reaction Processes at Individual Ag Nanoparticles by 3D Superlocalization Microscopy. Nano Lett. 15, 6454–6463 (2015).
2. Almeida, M. S. de, Susnik, E., Drasler, B., Taladriz-Blanco, P., Petri-Fink, A. & Rothen-Rutishauser, B. Understanding nanoparticle endocytosis to improve targeting strategies in nanomedicine. Chem. Soc. Rev. 50, 5397–5434 (2021).
3. Andrecka, J., Arroyo, J. O., Takagi, Y., de Wit, G., Fineberg, A., MacKinnon, L., Young, G., Sellers, J. R. & Kukura, P. Structural dynamics of myosin 5 during processive motion revealed by interferometric scattering microscopy. Elife 2015, (2015).
4. Gross, M., Verpillat, F. & Desbiolles, P. 3D localization and tracking of gold particles in biological environment using digital holography. BSu3A.62 (2013) doi:10.1364/biomed.2012.bsu3a.62.
5. Martinez-Marrades, A., Rupprecht, J.-F., Gross, M. & Tessier, G. Stochastic 3D optical mapping by holographic localization of Brownian scatterers. Opt. Express 22, 29191 (2014).
6. Bon, P., Bourg, N., Lécart, S., Monneret, S., Fort, E., Wenger, J. & Lévêque-Fort, S. Three-dimensional nanometre localization of nanoparticles to enhance super-resolution microscopy. Nat. Commun. 6, (2015).
7. Lombaert, H., Grady, L., Pennec, X., Ayache, N. & Cheriet, F. Spectral log-demons: Diffeomorphic image registration with very large deformations. Int. J. Comput. Vis. 107, 254–271 (2014).
8. Hajj, B., El Beheiry, M., Izeddin, I., Darzacq, X. & Dahan, M. Accessing the third dimension in localization-based super-resolution microscopy. Phys. Chem. Chem. Phys. 16, 16340–16348 (2014).
9. Kao, H. P. & Verkman, A. S. Tracking of single fluorescent particles in three dimensions: use of cylindrical optics to encode particle position. Biophys. J. 67, 1291–1300 (1994).
10. Huang, B., Wang, W., Bates, M. & Zhuang, X. Three-dimensional super-resolution imaging by stochastic optical reconstruction microscopy. Science (80-.). 319, 810–813 (2008).
11. Bon, P., Linarès-Loyez, J., Feyeux, M., Alessandri, K., Lounis, B., Nassoy, P. & Cognet, L. Self-interference 3D super-resolution microscopy for deep tissue investigations. Nat. Methods 15, 449–454 (2018).
12. Primot, J. & Sogno, L. Achromatic three-wave (or more) lateral shearing interferometer. J. Opt. Soc. Am. A 12, 2679 (1995).
13. Feng, S., Kane, C., Lee, P. A. & Stone, A. D. Correlations and fluctuations of coherent wave transmission through disordered media. Phys. Rev. Lett. 61, 834–837 (1988).
14. Wu, T., Katz, O., Shao, X. & Gigan, S. Single-shot diffraction-limited imaging through scattering layers via bispectrum analysis. Opt. Lett. 41, 5003 (2016).
15. Antipa, N., Kuo, G., Heckel, R., Mildenhall, B., Bostan, E., Ng, R. & Waller, L. DiffuserCam: lensless single-exposure 3D imaging. Optica 5, 1 (2018).
16. Linda Liu, F., Kuo, G., Antipa, N., Yanny, K. & Waller, L. Fourier DiffuserScope: single-shot 3D Fourier light field microscopy with a diffuser. Opt. Express 28, 28969 (2020).
17. Li, X., Stevens, A., Greenberg, J. A. & Gehm, M. E. Single-shot memory-effect video. Sci. Rep. 8, 1–8 (2018).
18. Berto, P., Rigneault, H. & Guillon, M. Wavefront sensing with a thin diffuser. Opt. Lett. 42, 5117 (2017).
19. Bon, P., Wattellier, B. & Monneret, S. Modeling quantitative phase image formation under tilted illuminations. Opt. Lett. 37, 1718 (2012).
20. Wang, C., Fu, Q., Dun, X. & Heidrich, W. Quantitative Phase and Intensity Microscopy Using Snapshot White Light Wavefront Sensing. Sci. Rep. 9, (2019).
21. N, P., M, M. & B, T. Pore size of agarose gels by atomic force microscopy. Electrophoresis 18, 55–58 (1997).
22. Khadir, S., Andrén, D., Chaumet, P. C., Monneret, S., Bonod, N., Käll, M., Sentenac, A. & Baffou, G. Full optical characterization of single nanoparticles using quantitative phase imaging. Optica 7, 243 (2020).
23. Sims, R. R., Abdul Rehman, S., Lenz, M. O., Benaissa, S. I., Bruggeman, E., Clark, A., Sanders, E. W., Ponjavic, A., Muresan, L., Lee, S. F. & O'Holleran, K. Single molecule light field microscopy. Optica 7, 1065 (2020).
24. Liebel, M., Arroyo, J. O., Beltrán, V. S., Osmond, J., Jo, A., Lee, H., Quidant, R. & van Hulst, N. F. 3D tracking of extracellular vesicles by holographic fluorescence imaging. Sci. Adv. 6, (2020).